MULTIFRACTAL PROPERTIES OF EVOLVING ACTIVE REGIONS

P. A. Conlon[1], P. T.Gallagher[1], R. T. J. McAteer[2], J. Ireland[3], C. A. Young[3], P. Kestener[4], R. J. Hewett[5], K. Maguire[6]
[1] *Astrophysics Research Group, School of Physics, Trinity College Dublin, Dublin 2, Ireland (*conlon.paul@gmail.com*).*
[2] *Catholic University of America, NASA Goddard Space Flight Center, Greenbelt, MD 20771, USA.*
[3] *ADNET Systems Inc., NASA Goddard Space Flight Center, Greenbelt, MD 20771, USA.*
[4] *DSM/DAPNIA/SEDI, CEA Saclay, ,Gif-sur-Yvette, France.*
[5] *Computer Science Departement, University of Illinois at Urbana-Champaign, Urbana, IL 61801,*
[6] *School of Physics, University College Dublin, Belfield, Dublin 4, Ireland.*

Received ; accepted

Abstract.
Magnetohydrodynamic turbulence is thought to be responsible for producing complex, multiscale field distributions in solar active regions. Here we explore the multiscale properties of a number of evolving active regions using magnetograms from the Michelson Doppler Imager (MDI) on the Solar and Heliospheric Observatory (SOHO). The multifractal spectrum was obtained using a modified box-counting method to study the relationship between magnetic field multifractality and region evolution and activity. The initial emergence of each active region was found to be accompanied by characteristic changes in the multfractal spectrum. Specifically, the range of multifractal structures (D_{div}) was found to increase during emergence, as was their significance or support (C_{dev}). Following this, a decrease in the range in multfractal structures occurred as the regions evolved to become large-scale, coherent structures. From the small sample considered, evidence was found for a direct relationship between the multifractal properties of the flaring r egions and their flaring rate.

Keywords: Sun: magnetic field, Turbulence, Fractals, Multifractals

1. Introduction

Solar active regions are complex concentrations of kilogauss magnetic fields in the solar photosphere. They are highly dynamic surface features and are the source of many extreme solar events, such as flares and coronal mass ejections (CMEs; Gallagher et al., 2006). One of the main goals of modern solar and space weather research is to understand the fundamental physics responsible for the evolution and activity of these regions.

Magnetic flux ropes are thought to be formed in the tachocline near the base of the Sun's convective zone (Miesch, 2005). Magnetic buoyancy cause these flux ropes to rise to the surface to form Ω-shaped loops (Abbett &

Fisher, 2003). Turbulent flows near the surface then cause these flux ropes to become twisted and distorted. As the flux ropes emerge into the corona, the decreasing atmospheric pressure causes the flux ropes to expand rapidly to form active region coronal loops. As the smaller scale flux ropes emerge, they coalesce to form larger scale structures (Aschwanden, 2005). The resulting magnetic flux distribution is found to exhibit self-similar properties consistent with a highly turbulence and non-linear formation process (McAteer, Gallagher & Ireland, 2005; Abramenko, 2005).

The motion of magnetic elements within active regions are governed by two processes: flux emergence and decay; and bulk mass motions. Using the magnetic induction equation, an expression for the magnetic Reynolds number of the form $R_m = LV/\eta$ can be obtained. Where L, V and η are the length scales, velocities and viscosity on the photosphere. For typical photospheric length-scales and velocities, the magnetic Reynolds number is $\sim 10^6 - 10^{10}$ (Parker, 1979). The photosphere is therefore highly turbulent and chaotic in nature.

Solar active regions have been shown to display power law distributions, identifying them as non-linear, coherent processes (Lu & Hamilton, 1991; Bak, 1996). The maintenance of a power law distribution points to self-organized criticality (SOC) in active region emergence. The SOC nature of active regions is a result of the turbulent nature of the flux tubes rooted in the photosphere. Under SOC the active regions buildup energy until some threshold is surpassed, and the energy is released as a flare. With the knowledge that the regions are highly chaotic, turbulent systems; tools from non-linear analysis can be applied to understand the dynamics behind these energy releases.

With this motivation, several authors have investigated the self-similar nature of solar active regions (Abramenko et al., 2002; Abramenko, 2005; Georgoulis, 2005; McAteer, Gallagher & Ireland, 2005; Lawrence & Cadavid & Ruzmaikin, 1996). They both calculated the fractal dimension of active region magnetic fields using two different methods: structure functions and boxcounting methods. (Abramenko et al., 2002; Abramenko, 2005) used several methods to extract parameters associated with the turbulent properties of a sample of active regions, and found a clear correlation between increased fractal dimension and flaring activity. A more extensive statistical study by McAteer, Gallagher & Ireland (2005) found that flaring activity was only weakly related to a region's fractal dimension.

To fully characterize the complexity of active region magnetic fields, methods that are sensitive to scale are therefore required. This allows for the detection and characterization of the distribution of magnetic flux within an active region. Georgoulis (2005) concluded that fractal and multifractal parameters involving scales across the measure space, had limited ability in space weather prediction. Conversely, Abramenko (2005) has shown the

power of multifractal methods to detect the difference between flaring and non-flaring regions.

In this paper, multifractal methods are used to analyze the distribution of magnetic flux in a number of evolving active regions observed using MDI. These observations are described in §2. In §3, the fractal and multifractal methods are discussed, while our results are given in §4. Our conclusions and future directions are then given in §5.

2. Observations and Data Reduction

Magnetic-field measurements were obtained by the MDI instrument, which images the Sun on a 1024×1024 pixel CCD camera through a series of increasingly narrow filters. The final elements, a pair of tunable Michelson interferometers, enable MDI to record filtergrams with an FWHM bandwidth of 94 mÅ. In this paper, 96-minute magnetograms of the full disc were used, which had a pixel size of ∼2".

For the purposes of this work, four active regions were analyzed as they evolved on the solar disk. NOAA 10727 emerged as a β region on 2005 January 24 and experienced significant flux emergence on the 29th, before rotating off the disk on 2005 February 3. NOAA 10763 rotated onto the disk on 2005 May 11 as a $\beta\gamma$ region. It subsequently formed a δ in its trailing portions and went into decay from 2005 May 16. The most active region in the sample was the rapidly emerging active regions, NOAA 10488. This region emerged on 2003 October 26 to become a $\beta\gamma\delta$ region on the subsequent day. The final region in the sample was NOAA 10798, which emerged on 2005 August 15, and slowly grew in size and complexity over a ten day period.

Flux densities were corrected using the algorithm suggested by Berger & Lites (2003) and implemented in Green et al. (2003). Magnetic field projection effects were corrected by assuming a radial field at each point on the solar disk and implementing a cosine-correction algorithm. Image projection effects were corrected using an equal-area cylindrical projection method (Bugayevskiy & Snyder 1995; McAteer et al. 2005).

3. Fractals & Multifractals

Classically the fractal dimension is calculated by covering an object with boxes of varying size ϵ. The fractal dimension of an object is given by the scaling relation:

$$N(\epsilon) \propto \epsilon^{-D}, \tag{1}$$

where D is the fractal dimension, and $N(\epsilon)$ is the number of boxes of size ϵ. Fractals give us insight into the complexity of objects that Euclidean analysis cannot.

Although fractals are useful for describing the complexity of images and regions, it has been found that most systems are a convolution of different fractal processes. To properly characterize such systems, the idea of a *multifractal* was introduced. Multifractals, like fractals, relate the number of boxes $N(\epsilon)$ to the size of each box ϵ and are characterized by a similar equations to Equation (1):

$$N(\epsilon) \propto \epsilon^{-f(\alpha)}, \tag{2}$$

where instead of a single exponent, there is a spectrum of exponents $f(\alpha)$ each with a relative strength or significance α. To extract the spectrum of exponents a moment q is used. When q is positive it magnifies the larger measures, dwarfing the smaller ones. The opposite happens when q is negative; it inverts the measure, thus enhancing the smaller measures and dwarfing the larger ones. The reader is referred to McAteer et al. (2007) for a detailed discussion of all the parameters.

Following Lawerence & Schijver (1993), the measure of the line-of-sight magnetograms is, $B_\epsilon(i)$, which is given by the field strength contained in box i of size ϵ. For line-of-sight magnetograms, oppositely signed field strength is allowed to cancel within a box and the magnitude is used. The normalized flux $\hat{B}_\epsilon(i)$ is then given by:

$$\widehat{B}_\epsilon(i) = \frac{B_\epsilon(i)^q}{\sum_{i=1}^{N(\epsilon)} B_\epsilon(i)^q} = \frac{B_\epsilon(i)^q}{z_\epsilon(q)}, \tag{3}$$

where $z_\epsilon(q) = \sum_{i=1}^{N(\epsilon)} B_\epsilon(i)^q$ is known as the partition function.

The strength or significance of a measure is then:

$$\alpha(q) = \lim_{\epsilon \to 0} \sum_{i=1}^{N(\epsilon)} \widehat{B}_\epsilon(i) \log_\epsilon B_\epsilon(i), \tag{4}$$

$$= \lim_{\epsilon \to 0} \sum_{i=1}^{N(\epsilon)} \widehat{B}_\epsilon(i) \alpha_\epsilon(i), \tag{5}$$

where $B_\epsilon(i) = \epsilon^\alpha$. $\alpha(q)$ measures the concentration strength of the range of measure scales given by q (Chappell & Scalo , 2001). For $\alpha = 2$ we have a two dimensional image, for a sharp spike $\alpha = 0$.

The distribution of all the points in the image of a given concentration strength is then given by $f(\alpha)$:

$$f(q) = \lim_{\epsilon \to 0} \sum_{i=1}^{N(\epsilon)} \widehat{B}_\epsilon(i) \log_\epsilon \widehat{B}_\epsilon(i), \tag{6}$$

$$f(\alpha) = q\alpha - \lim_{\epsilon \to 0} \sum_{i=1}^{N(\epsilon)} \widehat{B}_\epsilon(i) \log_\epsilon z_\epsilon(q), \quad (7)$$

$$= q\alpha - \tau, \quad (8)$$

where $\tau = \lim_{\epsilon \to 0} \log_\epsilon E(z_\epsilon(q))$. $f(\alpha)$ for $q = 0$ corresponds to the Hausdroff or fractal dimension.

The algorithm used was a modified box-counting method as developed by Mach & Mas (1997). The basic method involves covering the image in a grid with inter-grid spacing ϵ and counting the number of locations that contain part of the detail (Mandelbrot & Whitrow, 1983). A modification of this is to randomly sample the image and renormalize the calculations (Cadavid et al., 1994).

Due to errors in the calculation of the multifractal spectrum for negative q, we decided to characterize the changing complexity by only using the results for positive q (the poor resolution of the fine scale structures being enhanced by the discrete and numerical nature of the method). Following from the ideas of Chappell & Scalo (2001) we use the terms *contribution diversity* and *dimensional diversity* defined as:

$$C_{div} = \alpha_{max} - \alpha_{min}, \quad (9)$$

$$D_{div} = f(\alpha)_{max} - f(\alpha)_{min}, \text{ for } q > 0. \quad (10)$$

This allows us to parameterize changes in the system over time. A broadening of the spectrum would result from a decrease in the contribution of larger measures to an active region. While the region grows the larger measure will become more significant and the contribution diversity will increase.

4. Results

4.1. Theoretical Fractals

The methods described in § 3 were tested using a know fractal and multifractal. The Sierpinski carpet was chosen as the fractal for testing. This was constructed by covering the domain with a 3×3 grid and setting the middle section to zero. This process was continued until the smallest scale was reached (1 pixel). This created a self-similar image with a fractal dimension of $D = log(8)/log(3) \approx 1.8928$. The top left of Figure 1 shows an image of the Sierpinski carpet, and its corresponding theoretical singularity spectrum below. Using the methods outlined in the previous section, a point-like singularity spectrum with a fractal dimension of D or $f(\alpha) = 1.8932 \pm 0.01$ was obtained, with a corresponding value of $\alpha = 1.87 \pm 0.009$. A monofractal has the same fractal dimension at all scales with equal strength.

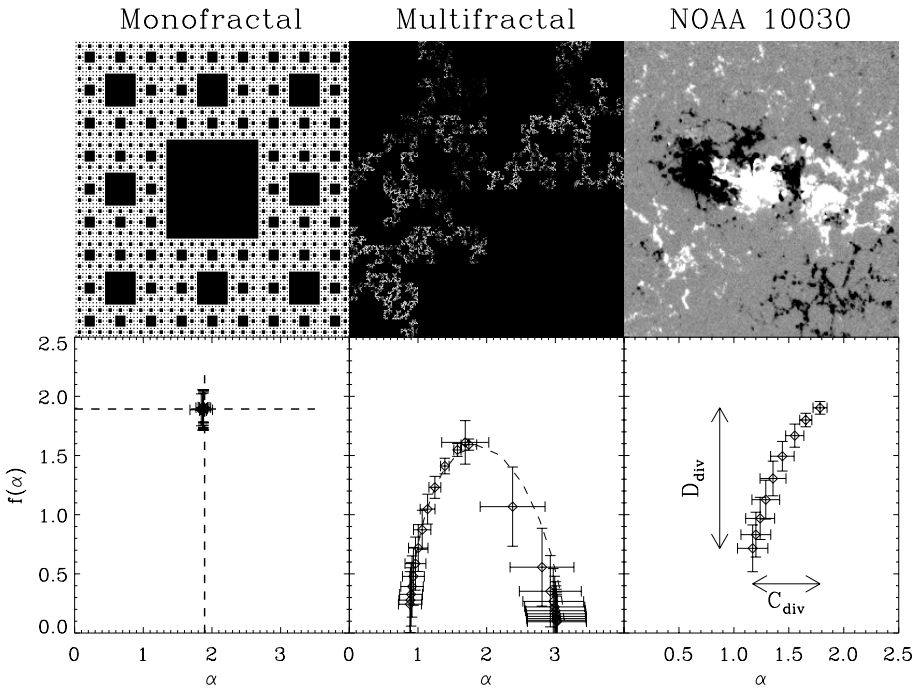

Figure 1. (Top) A monofractal image, multifractal image and magnetogram of NOAA 10486. The corresponding $f(\alpha)$ spectra are shown in the bottom panels.

A multifractal image and its theoretical singularity spectrum was created using the methods of Cadavid et al. (1994). The multifractal image is shown in the centre-top panel of Figure 1. Its corresponding theoretical spectrum (dashed lines) is given in the panel below. Also shown is the spectrum obtained using our methods. It can be seen that there is a good agreement between the theoretical and calculated spectra for $q > 0$ (i.e., the left-hand side of the spectrum). Results for the right side of the spectrum ($q < 0$) deviate due to errors in the discretization of the data and numerical issues with small measures. The final set of panels on the far right of Figure 1 show an MDI magnetogram for NOAA 10486. Its singularity spectrum is shown in the panel below. Due to the errors already mentioned, the left side of the spectrum ($q > 0$) could only be reliably calculated.

4.2. NOAA 10488

The evolution of the NOAA 10488 is shown in Figures 2 and 3. The region emerged rapidly over three days, starting on 26 October 2005. From Figure 2, the emergence was characterized by a significant change in the region's $f(\alpha)$ spectrum. Most notably, the contribution and dimension diversities becomes smaller as the region forms a large-scale coherent structure. This is

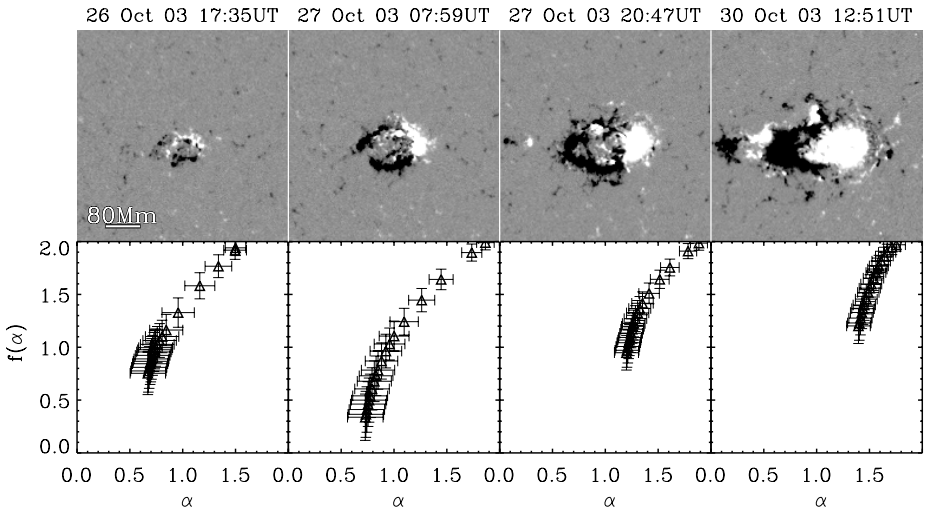

Figure 2. The emergence of NOAA 10488 on 26–30 October 2003. (Top) MDI magnetograms. (Bottom). The corresponding $f(\alpha)$ spectra.

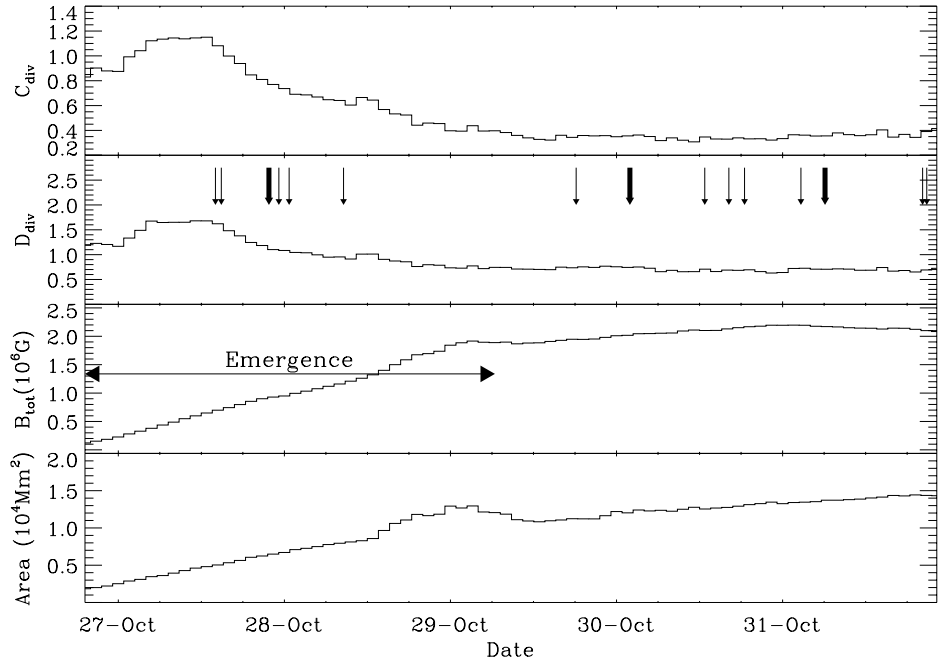

Figure 3. The evolution of NOAA 10488. (Top) Contribution diversity. (Second) Dimensional diversity. The total flux (gauss) and area (Mm) of the region are shown in the third and fourth panel respectively. Associated C-class flares are indicated by thin arrows, bolder arrows indicate M-class flares.

due to large field measures becoming more significant (i.e., moving to higher α) and more complex (i.e., moving to larger $f(\alpha)$).

Figure 3 shows the evolution of NOAA 10488's area, total flux, and contribution and dimensional contributions over five days, from 27 October to 1 November 2007. The initial flux emergence is characterized by a small increase in the multifractal parameters on 27 October 2005. This results from the emergence of isolated small-scale flux elements which subsequently coalesce to form a number of large-scale structures which have reduced significance. The multifractal properties of the region then remain constant for a number of hours as the region continues to grow in size and total flux.

At the end of 27 October 2003, the multifractal nature of the region again begins to change. Although the region continues to evolve rapidly, the contribution and diversity dimensions show a continued decrease, until reaching a plateau on 29 October 2005. This gradual decrease in D_{div} and C_{div} results from an increase in the significance and fractal dimension of larger scales as the region becomes a large-scale coherent active region. This gradual evolution of the region's multifractal properties is accompanied by an increase in the flaring activity of the region. The region then remains relatively stable from 29 October 2003 to 1 November 2003, during which the fractal properties of the region do not change significantly.

4.3. NOAA 10798

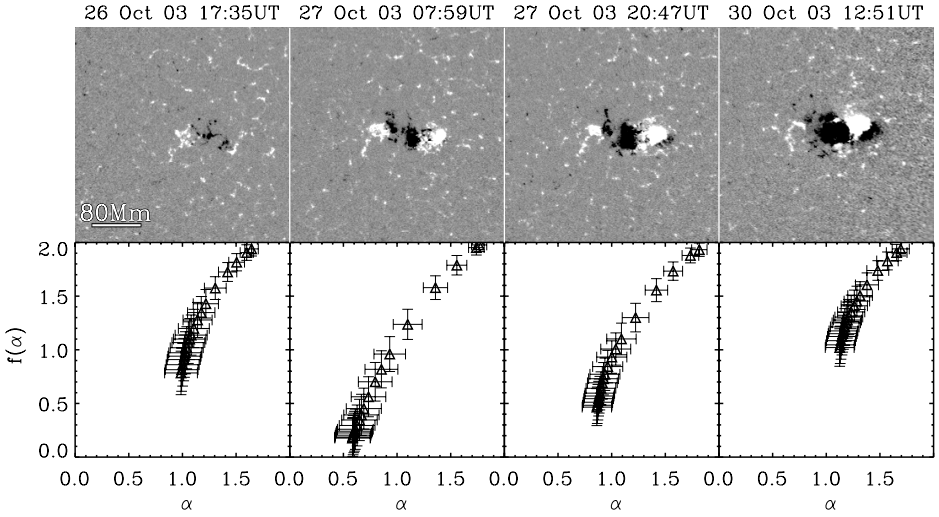

Figure 4. (Top) MDI magnetogram images of NOAA 10798 on 18-Aug-2005 04:47 UT, 18-Aug-2005 14:23 UT, and 19-Aug-2005 09:35 UT. (Bottom) The corresponding $f(\alpha)$ spectrum for each date.

The emergence of NOAA 10798 is seen in Figure 8 and 9. The initial emergence of flux is characterized by an increase in the contribution and dimensional diversity, due to the "dust" nature of the large flux elements at this time. Similarly to NOAA 10488, the contribution diversity and dimensional diversity decrease as the region develops a coherent structure. The region is observed to flare at 10:06 UT on 21 August 2005. This corresponds to an increased fractal dimension at larger scales.

4.4. NOAA 10763

The emergence of large scale flux in NOAA 10763 is shown in Figures 6 and 7. As the region grows from 19:15UT on 14 May 2005, an increase in the significance of the larger scales is seen (α_{min}). The dimensional diversity decrease over this time as the complexity of the larger scales increase from a dust like nature ($f(\alpha) \ll 1.0$) to a line like nature ($f(\alpha) \approx 1.0$). The region flares on 15 May 2005 17:35 UT. This corresponds to the formation of a coherent structure with increased fractal dimensions across all scales. An M3.5 flare is observed on 15 May 2005 22:27 UT. Unlike the emergence of flux in NOAA 10488 and 10798, an increase in the multifractal parameters is not present. The emergence in this case is in the center of an already de-

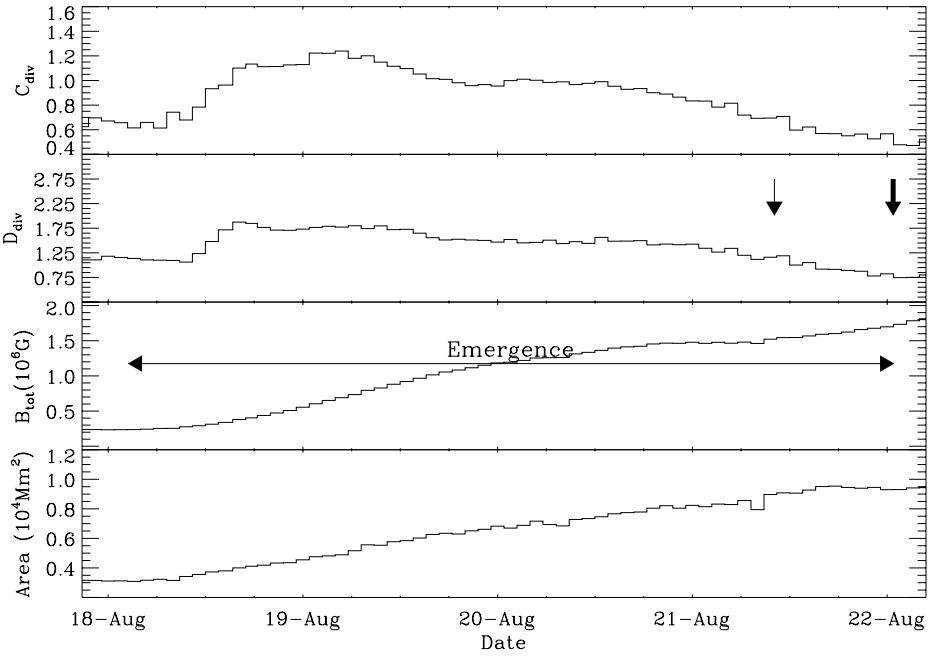

Figure 5. NOAA 10798: (top) contribution diversity, (second) dimensional diversity, (third) total flux (gauss) and (fourth) area (Mm). Associated C-class flares are indicated by thin arrows, bolder arrows indicate M-class flares.

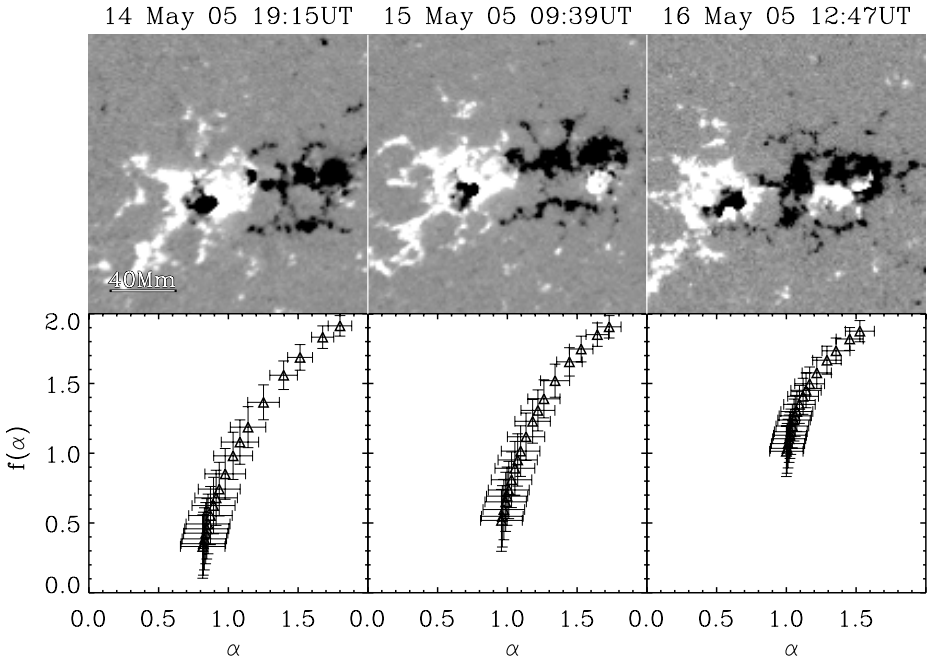

Figure 6. (Top) MDI magnetogram images for NOAA 10763 on 14-May-2005 19:15 UT, 15-May-2005 09:39 UT, and 16-May-2005 12:47 UT. (Bottom) $f(\alpha)$ spectra for each date.

veloped region. With this there is no initial increase in the contribution and dimensional diversity. Instead the multifractal parameters decrease steady as the larger scale flux elements grow in significance and complexity.

4.5. NOAA 10727

The formation of NOAA 10727 is shown in Figures 4 and 5. As flux elements emerge and form on the surface the peak of the singularity spectrum ($q = 0$) is seen to move to the right, Figure 4. This is due to the increased significance of the medium scales across the domain of interest. Similar to the formation of NOAA 10488, the emergence is characterized by an increase in the contribution diversity (C_{div}) and dimensional diversity (D_{div}) followed by a decrease in both parameters as the region forms a coherent structure. The emergence of additional large scale flux on 24 January 2005 is shown in Figure 5. The fractal dimension of larger scales ($f(\alpha_{min})$) are seen to decrease as the regions grow, a characteristic different from NOAA 10488. NOAA 10727 failed to flare during the time of observation, which may be due to the small fractal dimension of the larger scales ($f(\alpha_{min})$).

5. Discussion & Conclusions

The methods of §3 have been show to characterize the emergence of magnetic flux elements and the formation of active regions. The multifractal spectrum allows us to monitor the complexity and contribution across different scales. The emergence of large flux elements causes a change in the singularity spectrum, as the significance of larger flux is reduced relative to the preceding distribution. A decrease in the fractal dimension is also seen at the α_{min} region of the $f(\alpha)$ spectrum. As such, sudden changes in the multifractal parameters are excellent mathematical tool for detecting the emergence of solar magnetic fields.

We plan to investigate the multifractal method of these active regions further using the more stable Wavelet Modulus Maximum Methods (WTMM; Kestener & Arneodo (2004); McAteer et al. (2007)). This is a more stable method for extracting multifractal information. The use of wavelets as *fuzzy boxes* removes the errors inherent in the box counting method. Investigation into the negative q, small scale flux, will be possible with the increased stability of the WTMM method. With this, a more stable method for detecting changes in active regions will be possible. The investigation of additional

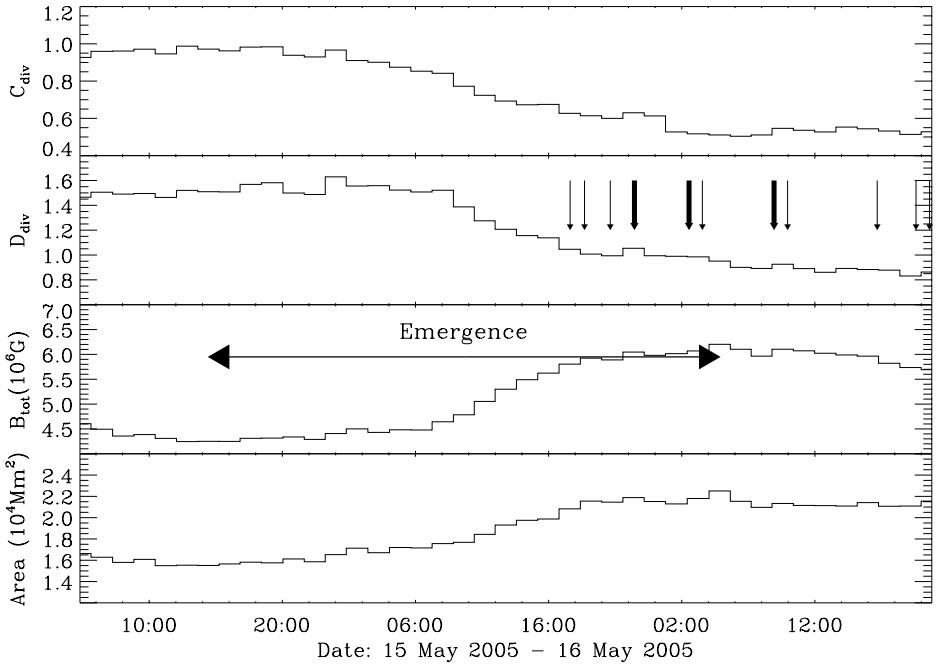

Figure 7. NOAA 10763. Contribution diversity (top) and dimensional diversity (second). Total flux (gauss) and area (Mm) are shown in third and fourth panels. Associated C-class flares are indicated by thin arrows, bolder arrows indicate M-class flares.

parameters from the WTMM method will increase our understanding of active region formation.

We have shown that the multifractal method provides a method for detecting the emergence of flux. This method by itself is incapable of detecting situations for the emergence of solar flares and CME's. Coupling this technique with the results of Hewett et al. (2007), into power law spacial scaling, would provide a more complete analysis tool. We plan to automate this method and incorporate it as a real-time feature on SolarMonitior (www.solarmonitor.org; Gallagher et al., 2002). This will allow for real time analysis for active regions changing magnetic topology.

Acknowledgements

The authors thank the SOHO/MDI consortia for their data. SOHO is a joint project by ESA and NASA. This work is supported by the NASA Living With a Star (LWS) program and the USAF European Office of Aerospace Research and Development. Paul Conlon is an Ussher Fellow at Trinity College Dublin. James McAteer is grateful to the NRC for the award of a research associateship for part of this work.

References

Abbett, W. P., & Fisher, G. H.: 2003, *Astrophys. J.*, **5**, 8.2, 475

Abramenko, V. I.: 2005, *Astrophys. J.*, **6**, 2.9, 1141

Abramenko, V. I.: 2005, *Solar Phys.*, **2**, 2.8, 29

Abramenko, V. I., Yurchyshyn, V. B., Wang, H., Spirock, T. J., & Goode, P. R.: 2002, *Astrophys. J.*, **5**, 7.7, 487

Alber, M. & Peinke J. : 1997, *Phys.Rev.E*, **57**, 5, 5489

Aschwanden, M. J.: 2005, Physics of the Solar Corona, Praxis Publishing Ltd, Chichester, UK.

Bak, P.: 1996, How nature works : the science of self-organized criticality / Per Bak. New York, NY, USA : Copernicus, c1996. QC173.4.C74 B34 1996,

Cadavid, A. C., Lawrence, J. K., Ruzmaikin, A. A., & Kayleng-Knight, A.: 1994, *Astrophys. J.*, **4**, 2.9, 391

Chappell, D., & Scalo, J.: 2001, *Astrophys. J.*, **5**, 5.1, 712

Davidson, P. A.: 2004, Turbulence : an introduction for scientists and engineers, by P.A. Davidson. Oxford, UK: Oxford University Press.

Gallagher, P. T. et al: 2006, Astrophysics And Space Science Library, 344, 1.2

Gallagher, P. T., Moon, Y.-J., & Wang, H.: 2002, *Solar Phys.*, **2**, 0.9, 171

Georgoulis, M. K.: 2005, *Solar Phys.*, **2**, 2.8, 5

Hewett et al., *Solar Phys.*, submitted

Lawrence, J. K.: 1991, *Solar Phys.*, **1**, 3.5, 249

Lawrence, J. K., & Schrijver, C. J.: 1993, *Astrophys. J.*, **4**, 1.1, 402

Lawrence, J. K., Cadavid, A. C., & Ruzmaikin, A. A.: 1996, *Astrophys. J.*, **4**, 6.5, 425

Lu, E. T., & Hamilton, R. J.: 1991, *Astrophys. Lett.*, **3**, 8.0, L89

Kestener, P., & Arneodo, A. 2004, Physical Review Letters, 93, 044501

Mach, J., & Mas, F.:1997, Physical Chemistry Dept., University of Barcelona, http://www.qf.ub.es/d2/jordi/mfrac.html

Mandelbrot, B. B., & Whitrow, G. J.: 1983, Journal of the British Astronomical Association, 93, 238

McAteer, R. T. J., Young, C. A., Ireland, J. & Gallagher P. T. : 2007,*Astrophys. J.* in press

McAteer, R. T. J., Gallagher, P. T., & Ireland, J.: 2005, *Astrophys. J.*, **6**, 3.1, 628

McAteer, R. T. J., Gallagher, P. T., Ireland, J., & Young, C. A.: 2005, *Solar Phys.*, **2**, 2.8, 55

Miesch, M. S., 2005, Living Rev. Solar Phys. 2.

Parker, E. N.: 1979, Oxford, Clarendon Press; New York, Oxford University Press, 1979, 858 p.,

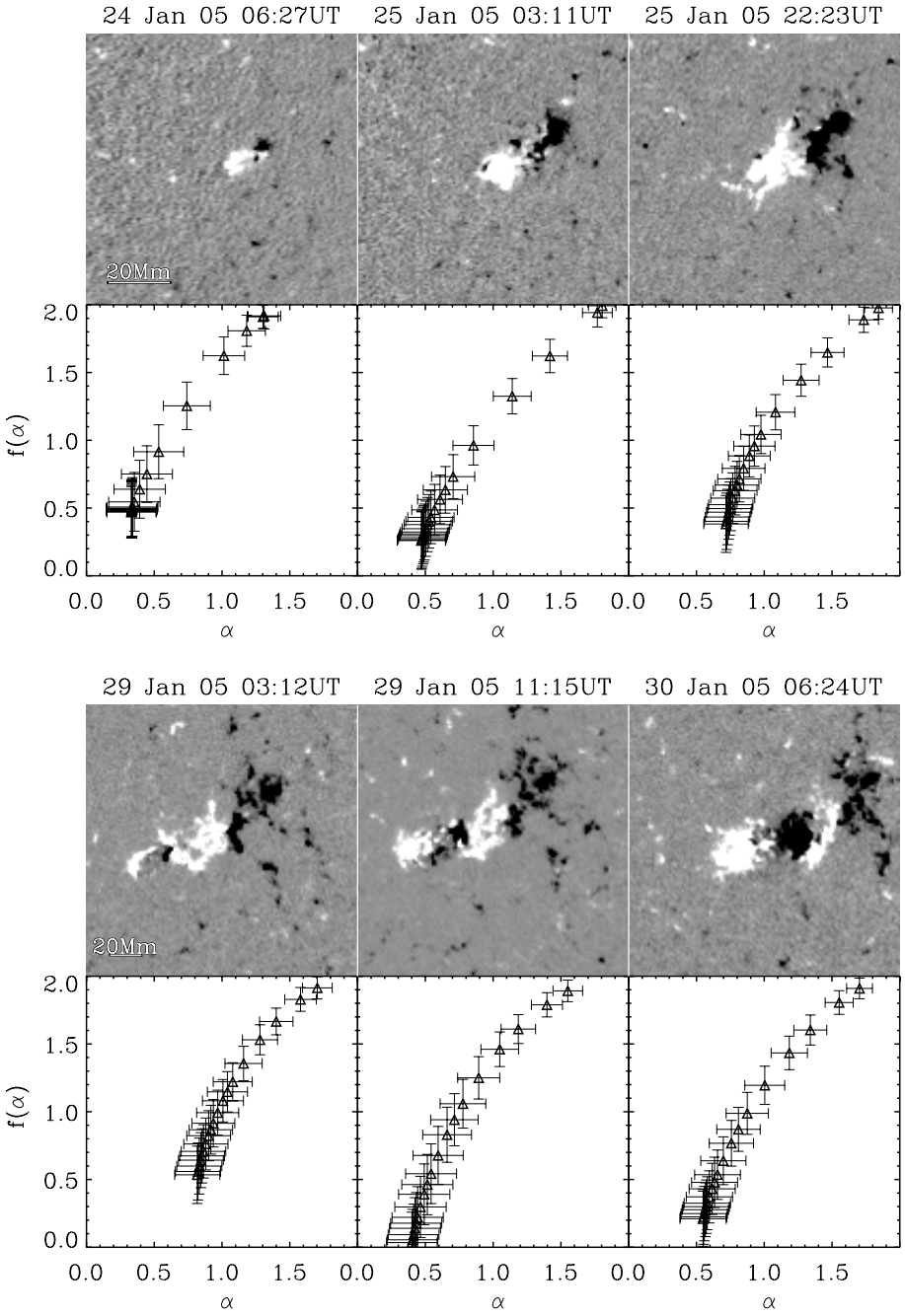

Figure 8. (Top) The emergence of NOAA 10727 MDI magnetogram on 2005 Jan. 24 06:27 UT, 2005 Jan. 24 03:11 UT, and 2005 Jan. 25 22:23 UT. (Second panel) The corresponding $f(\alpha)$ spectra for each image. (Third panel) MDI magnetogram on 2005 Jan. 29 03:12 UT, 2005 Jan. 29 11:15 UT and 2005 Jan. 30 06:24 UT. (Bottom) The $f(\alpha)$ spectra for each magnetograms.

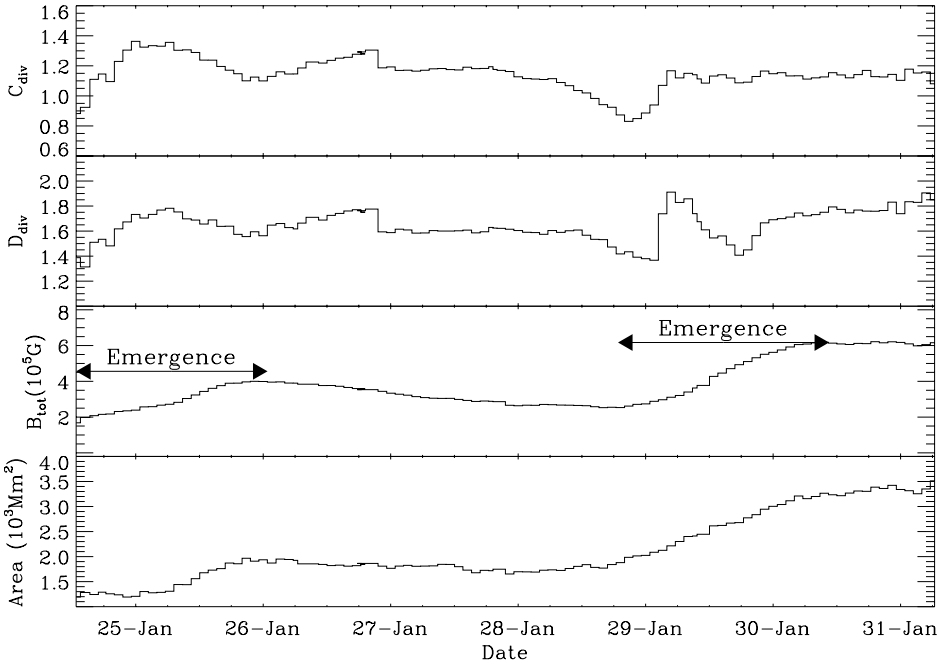

Figure 9. The evolution of NOAA 10727: Contribution diversity (top) and dimensional diversity (second). Total flux (gauss) and area (Mm) are shown in the third and fourth panels. There was no flares associated with NOAA 10727